JOC The Journal of Organic Chemistry

Article

pubs.acs.org/joc

Synthesis, Structure, Properties, and Bioimaging of a Fluorescent Nitrogen-Linked Bisbenzothiadiazole

Alberto A. R. Mota,[†] José R. Corrêa,[†] Pedro H. P. R. Carvalho,[†] Núbia M. P. de Sousa,[†] Heibbe C. B. de Oliveira,[†] Claudia C. Gatto,[†] Demétrio A. da Silva Filho,[‡] Aline L. de Oliveira,[†] and Brenno A. D. Neto*[,†]

[†]Laboratory of Medicinal and Technological Chemistry, University of Brasilia (IQ-UnB), Campus Universitário Darcy Ribeiro, CEP, P.O. Box 4478,Brasilia, DF 70904-970, Brazil

[‡]Institute of Physics, University of Brasilia (IF-UnB), Campus Universitario Darcy Ribeiro, CEP, Brasilia, DF 70919-970, Brazil

Supporting Information

ABSTRACT: This paper describes the synthesis, structure, photophysical properties, and bioimaging application of a novel 2,1,3-benzothiadiazole (BTD)-based rationally designed fluorophore. The capability of undergoing efficient stabilizing processes from the excited state allowed the novel BTD derivative to be used as a stable probe for bioimaging applications. No notable photobleaching effect or degradation could be observed during the experimental time period. Before the synthesis, the molecular architecture of the novel BTD derivative was evaluated by means of DFT calculations to validate the chosen design. Single-crystal X-ray analysis revealed the nearly flat characteristics of the structure in a *syn* conformation. The fluorophore was successfully tested as a live-cell-imaging probe and efficiently stained MCF-7 breast cancer cell lineages.

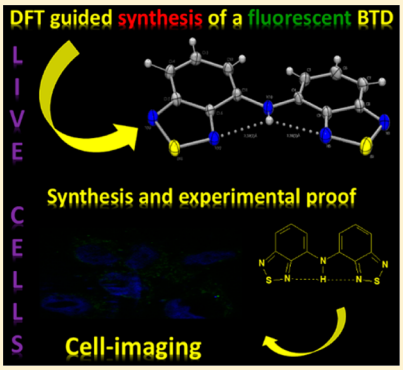

INTRODUCTION

The rational design of fluorescent bioprobes for cellular application is a challenging task.[1] Although fluorescent small-molecule technology dates back 150 years,[2] a real comprehension associating a specific molecular architecture and its cellular selection in the native cell environment is experiencing the first consolidated steps.[3] During the planning stage, it is necessary to take into account many principles that rule the rational design of novel selective cellular markers.[4] It is imperative for the new organic small molecule to display some chemical and photochemical features without which the successes of the probe will be compromised,[5] regardless the new probe proves to be capable of staining any of the possible cellular components or organelles. Currently, it is known that these new small-molecule bioprobes must indeed both meet strict requirements and display precise responses for specific stimulations inside a complex biological system.[6] The cellular environment contains a host of competing analytes that make the task even more challenging due to the uncountable possibilities of interactions and reactions, therefore requiring an "innocent" chemical behavior of the fluorophore.

High chemical stability in the excited state is, for instance, a feature of vital importance for fluorescent candidates, with the aim of promising biological applications.[6] Among some possible stabilizing processes, excited-state intramolecular proton transfer (ESIPT, Scheme 1)[7] prone fluorophores are, for example, found in a prominent position due to the fast H-transfer in the excited state, which lowers the energy of the system.[8−10] When

Scheme 1. General Mechanism of the Excited-State Intramolecular Proton Transfer Process[a]

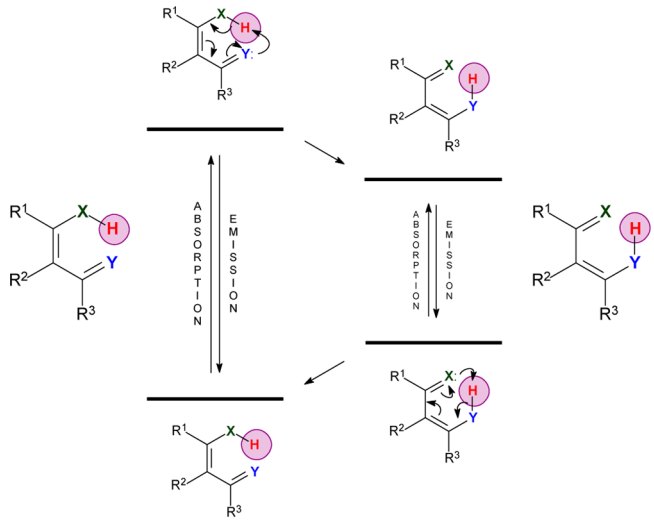

[a]X and Y represent general atoms and typically are nitrogen, oxygen, or sulfur.

Received: February 3, 2016
Published: March 1, 2016

DOI: 10.1021/acs.joc.6b00245
J. Org. Chem. 2016, 81, 2958−2965

the new fluorescent small molecule proves to be chemically and photophysically stable, it is then necessary to show its efficiency, stability, and biological innocence (without interfering with the cellular processes and homeostasis). The primary challenge is that the fluorophore must be capable of transposing the cell membrane, and for some, this is among the most desirable features for fluorogenic dyes.[11] Whether the new dye proves to be a cell-permeable fluorophore, which is difficult task,[12] it also has to be stable inside the cells and show no fading of its fluorescence emission during the cellular experiment. In other words, the bioprobe should not blink or degrade during the time taken to run the experiment.

In order to overcome all of these aforementioned drawbacks and challenges, and due to our interest in fluorescent bioprobes,[1,13−16] we aimed at designing and synthesizing a new fluorescent 2,1,3-benzothiadiazole (BTD) small-molecule derivative based on DFT predictions. In principle, this approach would allow for an evaluation of the new fluorophore structure/properties for further application in cell-imaging experiments using MCF-7 (breast cancer cells) as the cellular model in this work. BTDs are known for their high chemical stability[17] and photostability[15,18] and are being used as a new class of promising cellular markers.[1,14,19−21] Herein, we described the design, DFT calculations and predictions, synthesis, photophysical properties, X-ray and bioimaging experiments of a new fluorescent nitrogen-linked bis-BTD small molecule bearing two intramolecular H-bonds.

RESULTS AND DISCUSSION

The new fluorescent BTD derivative was produced using two commercially available compounds, as shown in Scheme 2. The Buchwald−Hartwig amination protocol together with an adaptation of a procedure previously described[22] was the used methodology to obtain the new compound (**BTDNHBTD**).

Scheme 2. Synthesis of the New Fluorescent BTD Derivative (BTDNHBTD)

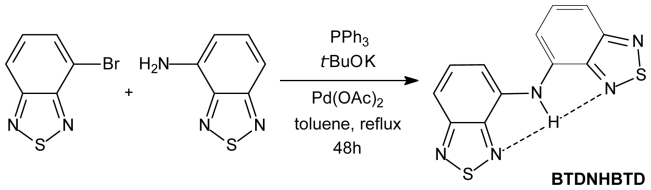

The design of the new compound was based on our experience on the development of fluorescent cellular markers bearing the BTD nucleus,[23−25] with the goal of stabilizing processes in the excited state, such as ESIPT or intramolecular charge transfer (ICT). Prior to the synthesis, however, DFT calculations were performed to verify whether the molecular architecture is appropriated and to predict the photophysical properties of the proposed structure in both the ground and excited states. The characterization of the new compound will be presented and discussed in due course. Theoretical approaches for studying fluorescent BTD derivatives that are capable of giving important insights into the design of the new structure have already been described to improve chemical and photophysical stabilities.[26−29] We have, for instance, investigated and proposed a rationale for the origin of single emission from a nonsymmetrical fluorescent atropisomeric BTD molecule, with excellent agreement between the theory and the experimental data.[24] We also have synthesized low HOMO−LUMO energy gap BTD derivatives based on DFT predictions.[30] In this sense, the new structure (**BTDNHBTD**) was rationally designed to display the following features:

(i) near flat structure toward an efficient π-conjugation[31] (and fluorescence emission)
(ii) two intramolecular H-bonds between the two BTD units linked by a conjugated nitrogen, targeting efficient ESIPT and/or ICT stabilizing processes[32]
(iii) rigid frame in the ground and excited states, considering the possibility of a strong geometric relaxation through an efficient ICT process[33,34]
(iv) chemical stability, which is inherently associated with the substituent groups and typical of π-extended BTD derivatives[35−45]
(v) direct and easy synthetic access to the new designed structure

In this context, the linkage of a second BTD unit through a direct cross-coupling reaction was thought to be ideal, as shown in Scheme 2. The designed **BTDNHBTD** would, in principle, fit all features expected for a new fluorophore for use as a new cellular marker.

DFT calculations were performed to obtain information concerning the orbital distribution (HOMO and LUMO plots), to depict electron density difference between the first excited and ground states, and to predict the extension of the stabilization after an ICT process (Figure 1). We also evaluated the absorption maxima (Figure 1) to visualize whether the structure would absorb above 400 nm to avoid any cellular autofluorescence emission in the cell-imaging experiments. Typically, fluorophores are excited up to 405 nm to guarantee no signal from autofluorescence of the cells. Geometry optimization interestingly afforded two possible low-energy conformations (named **BTDNHBTD-*syn*** and **BTDNHBTD-*anti***). The optimized geometries of two possible isomers for **BTDNHBTD** and their orbital maps as well as their electron density difference are presented in Figure 1. All calculations were performed at the PBE1PBE/6-311+G(2d,p)//CAM-B3LYP/6-311G(d) level of theory.

HOMO and LUMO orbitals were typically π-type, and LUMO centered on the BTD core, due to its electron-withdrawing properties and its capacity to act as a strong electron acceptor group. The electron density difference between the first excited and ground states ($\Delta\rho = \rho_{S1} - \rho_{S0}$) indicates the possibility of a robust geometric relaxation through an efficient ICT process. This relaxation provides an alternative interpretation, besides ESIPT, to the mechanism of excited-state deactivation in BTD derivatives.[46] ESIPT could not be completely ruled out, but the theoretical predictions indicate that the energy involved in the process is in agreement with an ICT stabilizing process.

Figure 1 (bottom, right) also shows the threshold absorption peak in the gas phase (black curves) and in water (red curves) for both isomers. To compute these spectra, the contributions from the two isomers (*syn* and *anti*) were considered with the same weight, being convoluted with Gaussian functions with fwhm equal to 20 nm. The contributions from each isomer were also plotted (*syn* with dashed lines and *anti* with dotted lines). In the gas phase, the shoulder that appears around 475 nm comes from the *anti* isomer. When we compared the relative position of the *syn* and *anti* transitions for water and the

DOI: 10.1021/acs.joc.6b00245
J. Org. Chem. 2016, 81, 2958−2965

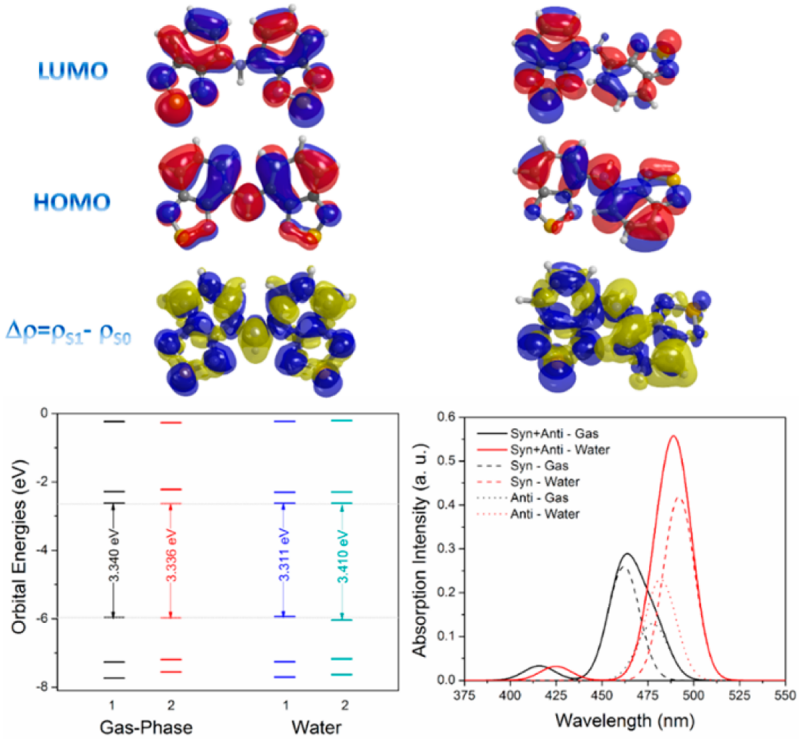

Figure 1. DFT calculations for both isomers of **BTDNHBTD** (*syn* on the left and *anti* on the right side) with optimized geometries. HOMO and LUMO plots are shown in blue and red. Electron density differences between the first excited and ground states ($\Delta\rho = \rho_{S1} - \rho_{S0}$) are shown in blue and yellow. Orbital energies are shown for both isomers (bottom, left) and predicted absorption spectra (bottom, right). All of these calculations were performed at the PBE1PBE/6-311+G(2d,p)//CAMB3LYP/6-311G(d) level of theory.

gas phase, it is clear that, in the gas phase, the *syn* isomer has higher energy than the *anti* isomer. The situation is inverted when the calculation is repeated using water as the solvent. It is possible to understand this inversion by looking at the charge distribution in both molecules (HOMO and LUMO plots; Figure 1). While in the *syn* isomer the dipole moment is along the short molecular axis, in the *anti* isomer, the dipole moment has sizable components along all three molecular axes. Thus, the presence of a protic and polar solvent promoted a higher stabilization of the *anti* isomer, leading to an inversion in the position of the transition energies of the two. Although the differences for both predicted structures are noted, both showed good stabilization possibilities from the excited state. This is an important feature than can be used in other bioimaging applications. Theoretical calculations also returned absorption maxima values above 400 nm, implying that bioprobes could also be irradiated at that region of the spectrum to avoid any cellular autofluorescence.

After the theoretical assessment of the designed **BTDNHBTD**, the new compound was indeed synthesized (as shown in Scheme 2) and fully characterized. **BTDNHBTD** afforded some suitable single crystals; therefore, the molecular structures could be also deduced from X-ray diffraction, as presented in Figure 2 (also see Figure S1 in the Supporting Information). Crystal and structure refinement data obtained for **BTDNHBTD** are summarized in Table 1.

It is depicted from the single-crystal X-ray diffraction that the two BTD rings are slightly twisted, with a dihedral angle of 26.6°, and only the *syn* isomer was detected in the crystal structure. Note also the two intramolecular H-bonds between N10—H10···N3 and N10—H10···N17 with distances of 2.360(3) and 2.390(3) Å, respectively. In a general way, the

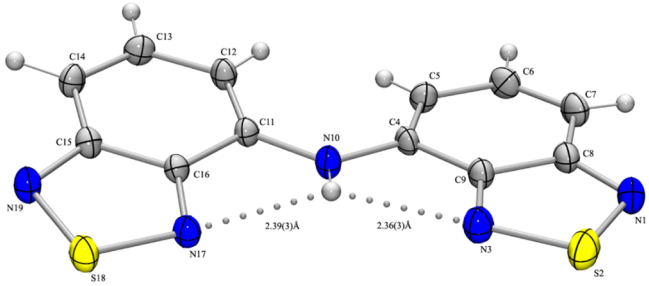

Figure 2. ORTEP-3 representation (30% probability displacement ellipsoids) of the asymmetric unit of **BTDNHBTD-*syn*** showing crystallographic labeling.

structures tend to be flat, and the intramolecular H-bond for N10—H10···N3 is found in the same plane of the BTD ring seen on the right side (Figure 2). This molecular architecture accounts for the occurrence of ESIPT processes to stabilize the structure in the excited state as a consequence of the good planarity observed for the **BTDNHBTD** derivative, as claimed for other derivatives[35] and analogues.[47] TD-DFT calculations, however, accounted for other stabilizing processes (ICT) instead of ESIPT.

As observed by looking along the *b* axis (Figure 3), the π—π interactions between BTD rings can be clearly identified. The interplanar distance of 2.530 Å (π-stacking) is typical for this kind of interaction.[48]

Interestingly, interactions between S···N of the BTD rings with distance of 3.114(3) Å form a tape-like network, as shown in Figure 4. These contacts have longer distances compared with those S···N interactions of 3.003(2) Å, previously reported for a BTD-NH-Ar derivative.[49] The results of X-ray diffraction

DOI: 10.1021/acs.joc.6b00245
J. Org. Chem. 2016, 81, 2958—2965

Table 1. X-ray Diffraction Data Collection and Refinement Parameters for BTDNHBTD

chemical formula	$C_{12}H_7N_5S_2$
M (g mol^{-1})	285.35
crystal system	monoclinic
space group	$P2_1/c$
unit cell	
a (Å)	11.642(7)
b (Å)	14.699(8)
c (Å)	6.942(4)
β	100.918(4)
V (Å^3)	1166.33(12)
Z	4
D_{calcd} (g cm^{-3})	1.625
index ranges	$-14 \le h \le 14$
	$-18 \le k \le 18$
	$-8 \le l \le 8$
absorption coefficient (mm^{-1})	0.447
absorption correction	multiscan
max/min transmission	0.9711/0.8646
measured reflections	12085
independent reflections/R_{int}	2398/0.0616
refined parameters	200
$R1$ (F)/$wR2$ (F^2) $(I > 2s(I))$	0.0457/0.0966
GoF	1.039
largest diff. peak and hole (e Å^{-3})	0.286 and −0.372
deposit number CCDC	970374

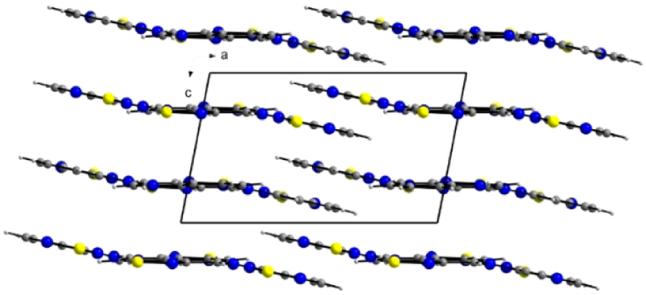

Figure 3. π-Stacking interactions observed in the packing of **BTDNHBTD-*syn*** viewed along the b axis.

analysis reveal intramolecular hydrogen bonds N10−H10···N3 [d(N···N) = 2.766(3) Å, ∠N10−H10···N3) = 116(3)°] and N10−H10···N17 [d(N···N) = 2.775(3) Å, ∠(N10−H10···N17) = 113(3)°] and S···N interactions affording two-dimensional intra- and intermolecular interaction networks for the **BTDNHBTD** structure.

NMR experiments were also conducted to investigate the existence of the two isomers in solution. $CDCl_3$, DMSO-d_6, and CD_3OD were initially used to probe the presence of the two theoretically predicted isomers. For all tested solvents, the presence of the two isomers could be observed in both ^{1}H (Figures S2−S4 in the Supporting Information) and ^{13}C NMR (Figures S5 and S6). NOESY experiments have also been performed in $CDCl_3$ to help identify these isomers (Figure S7 and S8). Note that there are six signals for carbons of the *syn* isomer and 12 for the *anti* isomer, as expected.

To determine the energetic barrier[50] between the two isomers, we followed the coalescence of the two amine signals upon increasing the temperature of DMSO-d_6 solution, varying the temperature from 20 to 150 °C (Figure 5). Figure S9 shows

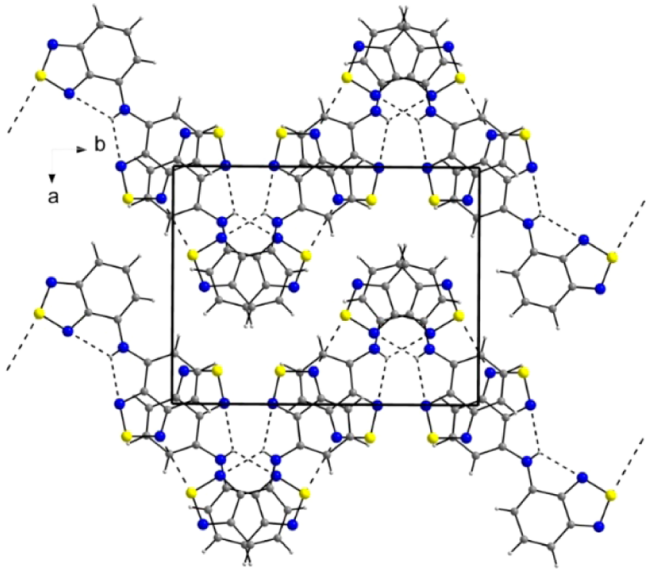

Figure 4. Crystal structure of **BTDNHBTD-*syn*** viewed along the c axis. Dotted lines show the S···N contacts and intramolecular H-bonds. Note the zigzag pattern formed by the chains along the b axis.

the full range spectra of the temperature variation experiment, and Table S1 lists the calculated values for the two isomers.

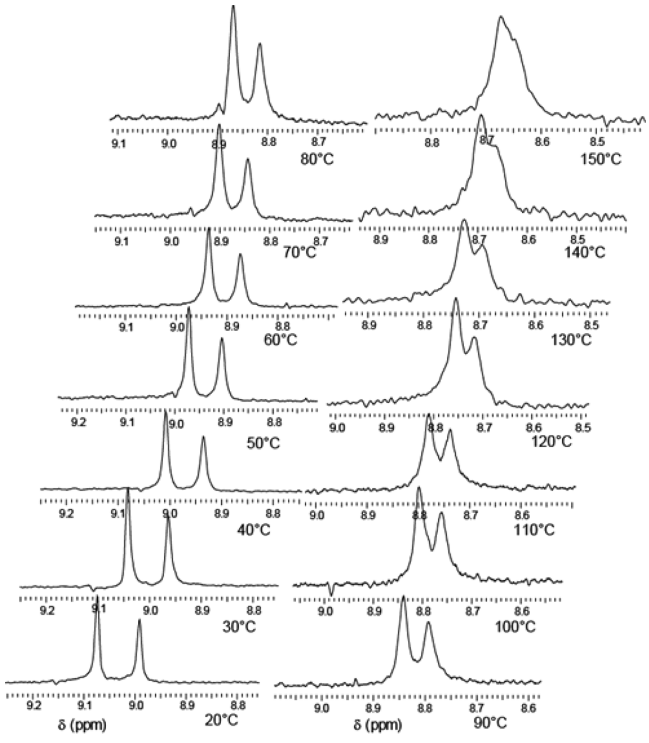

Figure 5. Temperature dependence of the ^{1}H NMR amine signal (300 MHz, DMSO-d_6) of **BTDNHBTD** isomers.

At the coalescence temperature (140 °C), the frequency of change of the isomers is given by

$$k_t = \frac{\pi(\Delta n)}{\sqrt{2}} \quad (1)$$

where k_t is the exchange constant and Δn is the distance between the signals (in ppm). For **BTDNHBTD**'s signals, k_t =

DOI: 10.1021/acs.joc.6b00245
J. Org. Chem. 2016, 81, 2958−2965

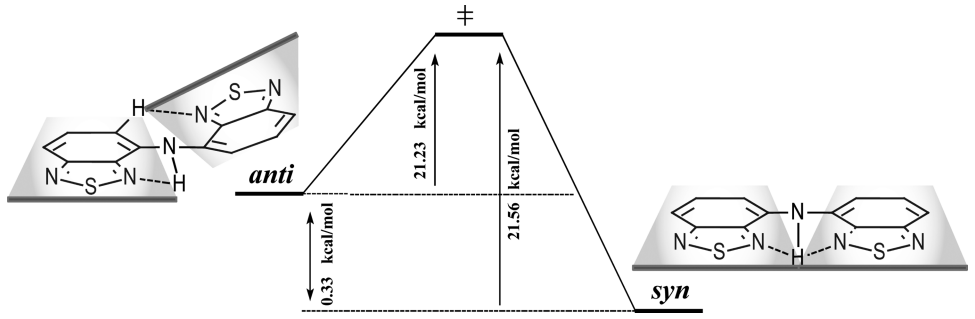

Figure 6. BTDNHBTD isomers and relative energies (kcal mol^{-1}). The *syn* isomer was considered to be the reference (0.00 kcal mol^{-1}).

59.94 Hz is found. This result shows that, at the coalescence temperature (140 °C), isomer interconversion (*syn* ↔ *anti*) is occurring at a frequency of approximately 60 Hz. The values of the free energies of activation ($\Delta G^{\#}$) of each isomer could be obtained using Eyring's equations as follows.

$$\Delta G_A^{\#} = RT_c \ln\left[\frac{k_B}{h\pi}\left(\frac{T_c}{\delta\nu}\right)\left(\frac{X}{1-\Delta P}\right)\right] \quad (2a)$$

$$\Delta G_B^{\#} = RT_c \ln\left[\frac{k_B}{h\pi}\left(\frac{T_c}{\delta\nu}\right)\left(\frac{X}{1+\Delta P}\right)\right] \quad (2b)$$

In eqs 2a and 2b, k_B (3.299×10^{-27} mol kcal K^{-1}), h (1.584×10^{-37} kcal s), and R (1.986×10^{-3} kcal mol^{-1}) are, respectively, the Boltzmann, Planck, and the universal ideal gas constants; $\delta\nu$ (Hz) is the difference between the isomer signals during the slow exchange process; ΔP is the difference between the molar fractions of the species; T_c is the coalescence temperature (°C), and X is a parameter which may be iteratively obtained through eq 3.

$$\Delta P = \left(\frac{X^2-2}{3}\right)^{3/2} \times \frac{1}{X} \quad (3)$$

At room temperature, it is depicted a mixture of 0.6:0.4 (*syn*:*anti*) indicating the integral area of the ^{1}H NMR could be directly used to measure their proportions. ΔP was determined as 0.2 for the two predicted and observed isomers of **BTDNHBTD**. The population of *anti* isomer increases with the increase of temperature. At 140 °C, the signals coalesced, indicating the free rotation for the interconversion of both isomers. The energy difference between the *syn* and *anti* isomers was only 0.33 kcal mol^{-1}. The interconversion barrier energies were 21.56 kcal mol^{-1} (*syn* → *anti*) and 21.23 kcal mol^{-1} (*anti*→ *syn*), respectively (Figure 6).

Theoretical calculations, performed at M062X/6-311+G-(2d,p), also allowed for an association between the energetic barriers and the solvents' dielectric constants (Figure S10). As depicted in Figure S10, it is possible to mathematically model these barriers as shown.

$$B_{forward}\ (\text{kcal mol}^{-1}) = 2.83 + 0.70e^{-0.11\varepsilon} \quad (4)$$

$$B_{reverse}\ (\text{kcal mol}^{-1}) = 1.03 - 0.13e^{-0.05\varepsilon} \quad (5)$$

where ε is the dielectric constant of the solvent. These results point firmly to the importance of solvent effects on the molecule stabilization in both the ground and excited states. In this sense, a significant solvatochromic effect is expected during the photophysical analyses.

After all structural characterizations, the fluorescent compound **BTDNHBTD** then had its photophysical properties characterized by means of spectrophotometric and spectrofluorometric analyses. The results are summarized in Table 2 and presented in Figure 7.

Table 2. UV−Vis and Fluorescence Emission Data (in Different Solvents) for BTDNHBTD

solvents	λ_{max} abs (nm)	log ε	λ_{max} em (nm)	Stokes shift (nm)
dimethylsulfoxide	455	3.57	586	131
water	458	3.40	607	149
ethyl acetate	447	3.62	549	102
dichloromethane	452	3.68	553	101
acetonitrile	447	3.56	575	128
toluene	457	3.66	521	64
ethanol	451	3.59	556	105
acetone	449	3.79	567	118
chloroform	455	3.71	541	86

The **BTDNHBTD** dye clearly exhibits large Stokes shifts, with values ranging from 64 to 189 nm (but typically up to 100 nm), commonly observed for fluorophores that undergo ESIPT. Independently of the solvent, the lowest energy absorption bands are assigned to characteristic $\pi-\pi^*$ transitions, by virtue of their large molar extinction coefficients (log ε values in the range of 3.40−3.68 mM^{-1} cm^{-1}), which is a characteristic associated with the spectroscopic signature of ESIPT processes.[51] The observed large Stokes shifts also suggest a structural change between the ground and excited states.[52] This suggests the possibility of H-transfer (ESIPT) in the excited state, as the observed structural changes are, in principle, in accordance with the ultrafast ESIPT from the Franck−Condon state.[53] With the data obtained by spectrophotometric and spectrofluorometric analyses, it was possible to describe the solvent effects in the first excited state. This was done by using the microscopic solvent polarity parameters (E_T^N) in the solvatochromic method.[54] E_T^N values provided by Reichardt[55] (Figure S11) have been used.

Despite all features firmly indicating an efficient ESIPT (*i.e.*, (i) a nearly flat structure with two strong H-bonds; (ii) large Stokes shifts; and (iii) intramolecular charge transfer nature for the electronic transitions), the theoretical calculations seem to correctly indicate that ICT is the main stabilizing process. Figure S11 shows the major role of ICT as the stabilizing process due to its R^2 value (0.52).[54] It is not possible to completely rule out the possibility of ESIPT, though. However, based on this value of R^2, the photophysical data (in accordance with DFT predictions) suggest that ICT is happening from the

DOI: 10.1021/acs.joc.6b00245
J. Org. Chem. 2016, 81, 2958−2965

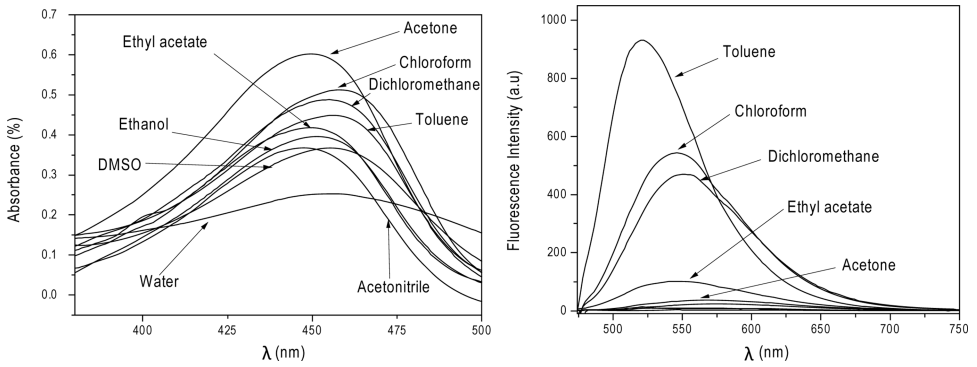

Figure 7. (Left) UV−vis absorption and (right) fluorescence spectra of **BTDNHBTD** in different solvents (concentration = 10 μM for all analyses).

first excited state of **BTDNHBTD**. In this context, the observed Stokes shifts are a reflex of both the dipole moment change of **BTDNHBTD** upon photoexcitation and also of the high stability of the fluorophore, in agreement with all of the photophysical data. As observed in Figures 1 and S10, these results are also in accord with the theoretically predicted importance of the solvent effect on the stabilization of **BTDNHBTD** in solution. Theoretical predictions had also indicated that the *anti* isomer is more stable in polar solvents; therefore, the dipole moment change could be somehow predicted, and the experimental data proved to be in good agreement with the data from the calculations.

Finally, to assess the potential application of the highly luminescent compound as a visible bioimaging probe, cell-imaging experiments were performed. MCF-7 cell lineages (breast cancer cells) were used as a cellular model. MCF-7 cells were submitted to staining procedures with **BTDNHBTD** (green) and commercially available DAPI (blue). Results are shown in Figure 8.

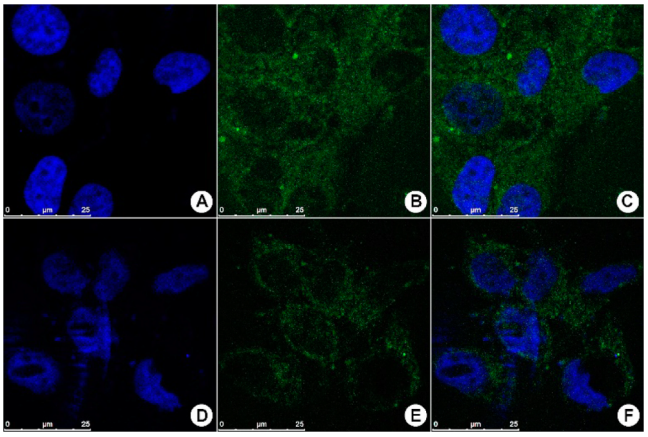

Figure 8. MCF-7 cells stained with **BTDNHBTD** and/or DAPI. (A−C) Fixed samples and (D−F) show fresh samples (live cells). (C,F) Merged images. The fluorescence staining pattern for **BTDNHBTD** is shown in green. The nucleus of the cells was stained with commercially available DAPI (blue). Scale bar = 25 μm.

The fluorophore was capable of transposing the cell membrane while sustaining its fluorescence emission (green), with no notable fading or blinking during the experimental time period. **BTDNHBTD** was found exclusively in the cytoplasm of the MCF-7 cells, showing high photostability, therefore rendering it suitable for further biological studies. The compound could not be observed inside the nuclei of the cells, thus indicating no affinity for nuclear components. The nuclear DNA was stained with commercially available DAPI (blue emission), and no interferences were noted by using both dyes. The results also show that **BTDNHBTD** could be used to stain either fixed or live cells.

CONCLUSIONS

In summary, the design, synthesis, characterization, and application of a novel fluorescent BTD has been achieved. The new compound (**BTDNHBTD**) proved to exist as two isomers almost in the same proportion at room temperature. Both isomers, however, showed high stability in the excited state, and ICT seems to be the major stabilizing process, although the possibility of ESIPT could not be completely ruled out. Theoretical calculations proved to be an outstanding tool for the prediction of the photophysical properties and molecular structure of the novel compound. X-ray analysis revealed the preference of the *syn* isomer in the solid state. Solution studies (NMR and photophysics) showed the coexistence of the two isomers in solution, which were predicted by the in silico approach. Cell-imaging experiments proved the potential of the new compound as a cellular marker, and it could be used alongside DAPI for multicolor cellular analyses. Additional biological experiments are underway and will be published elsewhere.

EXPERIMENTAL SECTION

General. Theoretical treatment of **BTDNHBTD** (both *syn* and *anti* isomers) was performed using the DFT approach of the Gaussian 09 program suite. Geometry optimization of the ground (S_0) state (in gas phase and water) was carried out with Pople's 6-311G(d) split-valence basis set and hybrid exchange−correlation functional, using the Coulomb attenuating method (CAMB3LYP). Harmonic frequency calculations were performed to verify whether we had located a genuine minimum. The optimized geometries of S_0 (both isomers) were used for the single-point TD-DFT calculation at the PBE1PBE/6-311+G(2d,p) level. The computed absorption spectra, in close agreement with experiments, were obtained at the TD-PBE1PBE/6-311+G(2d,p) level of calculation for both **BTDNHBTD** isomers. To compute the absorption spectra, contributions from both isomers were considered with the same weight, all being convoluted with Gaussian functions with fwhm equal to 20 nm. To include the solvent effects in our quantum mechanics calculations, we employed the self-consistent reaction field approach with the polarizable continuum model, in which the solute molecule was enclosed in a cavity embedded in a dielectric medium. All energy barrier height calculations for the interconversion between the two isomers (*anti* and *syn*) were performed at the M062X/6-311+G(2d,p) level of theory. NMR spectra were recorded on a 7.05 T instrument using a 5 mm internal diameter probe operating at 300 MHz for ^{1}H and at 75 MHz for ^{13}C.

DOI: 10.1021/acs.joc.6b00245
J. Org. Chem. 2016, 81, 2958−2965

Chemical shifts were expressed in parts per million (ppm) and referenced by the signals of the residual hydrogen atoms of the deuterated solvents, as indicated in the legends. Investigative temperature experiments were performed in a sealed NMR tube charged with DMSO-d_6. Breast cancer lineage (MCF-7) cells were seeded on coverslips at the bottom of 24-well plates and maintained on DMEM medium supplemented with 10% fetal calf serum at 37 °C in 5% CO_2 atmosphere. After 24 h, the cells were separated into two different groups: (1) cells incubated in fixative agents before the staining procedures and (2) cells submitted to staining procedures without the fixation step. All samples were washed three times with phosphate buffer saline (PBS, pH 7.4) at room temperature for 5 min each. The cells belonging to group (1) were fixed for 30 min in formaldehyde (3.7%) at room temperature and washed three times with PBS (5 min each) at room temperature. The cells belonging to group (2) were washed three times with the same conditions of group (1). The two groups of cells were incubated with **BTDNHBTD** (10 μM) for 30 min at room temperature. The cell samples were then washed three times in PBS at the same condition described above, and the nucleus could therefore be stained with DAPI according to the manufacturer's recommendations. The samples were mounted on glass slides using ProLong gold reagents. The cell images were acquired by using confocal laser scanning microscope (TCS SP5). The assays were performed in triplicate, and the tests were also performed three times.

General Procedure for the Synthesis of BTDNHBTD. In a Schlenk tube under N_2 atmosphere were added 214 mg (1.00 mmol) of 4-bromo-2,1,3-benzothiadiazole, 151 mg (1.0 mmol) of 4-amino-2,1,3-benzothiadiazole, 5 mol % of $Pd(OAc)_2$ (0.05 mmol, ca. 11 mg), 10 mol % of PPh_3 (0.1 mmol, ca. 26 mg), ^{t}BuOK (2.0 mmol, 224 mg), and 4 mL of anhydrous toluene. The mixture was kept at 100 °C under stirring for 72 h. The crude was filtered with Celite, and AcOEt was used as the eluent. The solvent was removed and the crude chromatographed using hexane/ethyl acetate (2:1 v/v). The desired compound was obtained in 40% yield (115 mg) as a crystalline solid.

Bis[4-(2,1,3-benzothiadiazole)]amine (BTDNHBTD): ^{1}H NMR ($CDCl_3$, 600 MHz) δ ppm 8.69 (br, 1H), 8.63 (br, 1H), 7.80 (d, J = 8.0 Hz, 1H), 7.65−7.45 (m, 7H), 7.43 (d, J = 7.7 Hz, 1H); ^{13}C NMR ($CDCl_3$, 150 MHz) δ ppm 155.5(7), 155.5(3), 153.5, 148.8(6), 148.8(0), 148.5, 133.5, 133.2(3), 133.2(0), 133.1, 130.9, 130.8, 113.7, 113.1, 108.8(7), 108.8(5), 108.3, 103.4; FT- IR (KBr, cm^{-1}) 3319, 3094, 3061, 2917, 2848, 1718, 1615, 1530, 1383, 830; mp 152−153 °C. Anal. Calcd for $C_{12}H_7N_5S_2$: C, 50.51; H, 2.47; N, 24.54. Found: C, 50.59; H, 2.59; N, 24.65.

■ ASSOCIATED CONTENT

Supporting Information

The Supporting Information is available free of charge on the ACS Publications website at DOI: 10.1021/acs.joc.6b00245.

NMR spectra and data from solution experiments, ORTEP representation of the single-crystal X-ray analysis, solvatochromic effects using the microscopic solvent polarity parameters, Cartesian coordinates for the calculated structures, and energy and thermal corrections (PDF)

Single-crystal X-ray analysis of **BTDNHBTD** (CIF)

■ AUTHOR INFORMATION

Corresponding Author

*E-mail: brenno.ipi@gmail.com. Fax: (+) 55 (61) 32734149. Phone: (+)55 (61) 31073867.

Notes

The authors declare no competing financial interest.

■ ACKNOWLEDGMENTS

This work was supported by CAPES, CNPq, FINEP-MCT, FINATEC, FAPDF, and DPP-UnB. B.A.D.N. also thanks the INCT-Catalysis and INCT-Transcend group. LNLS is acknowledge for the use of the facilities. D.A.S.F. gratefully acknowledges the financial support from the Brazilian Research Councils CNPq (Grant 306968/2013-4) and FAP-DF (Grant 0193.001.062/2015).

■ REFERENCES

(1) Neto, B. A. D.; Correa, J. R.; Silva, R. G. *RSC Adv.* **2013**, *3*, 5291−5301.
(2) Terai, T.; Nagano, T. *Pfluegers Arch.* **2013**, *465*, 347−359.
(3) Xu, Z.; Xu, L. *Chem. Commun.* **2016**, *52*, 1094−1119.
(4) Lavis, L. D.; Raines, R. T. *ACS Chem. Biol.* **2014**, *9*, 855−866.
(5) Yuan, L.; Lin, W. Y.; Zheng, K. B.; Zhu, S. S. *Acc. Chem. Res.* **2013**, *46*, 1462−1473.
(6) Chan, J.; Dodani, S. C.; Chang, C. J. *Nat. Chem.* **2012**, *4*, 973−984.
(7) Sun, W. H.; Li, S. Y.; Hu, R.; Qian, Y.; Wang, S. Q.; Yang, G. Q. *J. Phys. Chem. A* **2009**, *113*, 5888−5895.
(8) Rodembusch, F. S.; Leusin, F. P.; Bordignon, L. B.; Gallas, M. R.; Stefani, V. *J. Photochem. Photobiol., A* **2005**, *173*, 81−92.
(9) Cardoso, M. B.; Samios, D.; da Silveira, N. P.; Rodembusch, F. S.; Stefani, V. *Photochem. Photobiol. Sci.* **2007**, *6*, 99−102.
(10) Coelho, F. L.; Rodembusch, F. S.; Campo, L. F. *Dyes Pigm.* **2014**, *110*, 134−142.
(11) Nadler, A.; Schultz, C. *Angew. Chem., Int. Ed.* **2013**, *52*, 2408−2410.
(12) Guo, D. L.; Chen, T.; Ye, D. J.; Xu, J. Y.; Jiang, H. L.; Chen, K. X.; Wang, H.; Liu, H. *Org. Lett.* **2011**, *13*, 2884−2887.
(13) Diniz, J. R.; Correa, J. R.; Moreira, D. d. A.; Fontenele, R. S.; de Oliveira, A. L.; Abdelnur, P. V.; Dutra, J. D. L.; Freire, R. O.; Rodrigues, M. O.; Neto, B. A. D. *Inorg. Chem.* **2013**, *52*, 10199−10205.
(14) Neto, B. A. D.; Carvalho, P. H. P. R.; Correa, J. R. *Acc. Chem. Res.* **2015**, *48*, 1560−1569.
(15) Neto, B. A. D.; Lapis, A. A. M.; da Silva Júnior, E. N.; Dupont, J. *Eur. J. Org. Chem.* **2013**, *2013*, 228−255.
(16) Carvalho, P. H. P. R.; Correa, J. R.; Guido, B. C.; Gatto, C. C.; De Oliveira, H. C. B.; Soares, T. A.; Neto, B. A. D. *Chem. - Eur. J.* **2014**, *20*, 15360−15374.
(17) Moro, A. V.; Ferreira, P. C.; Migowski, P.; Rodembusch, F. S.; Dupont, J.; Ludtke, D. S. *Tetrahedron* **2013**, *69*, 201−206.
(18) Westrup, J. L.; Oenning, L. W.; da Silva Paula, M. M.; da Costa Duarte, R.; Rodembusch, F. S.; Frizon, T. E. A.; da Silva, L.; Dal-Bó, A. G. *Dyes Pigm.* **2016**, *126*, 209−217.
(19) Garcia, L.; Lazzaretti, M.; Diguet, A.; Mussi, F.; Bisceglie, F.; Xie, J.; Pelosi, G.; Buschini, A.; Baigl, D.; Policar, C. *New J. Chem.* **2013**, *37*, 3030−3034.
(20) Jiang, Q.; Zhang, Z.; Lu, J.; Huang, Y.; Lu, Z.; Tan, Y.; Jiang, Q. *Bioorg. Med. Chem.* **2013**, *21*, 7735−7741.
(21) Tian, Y. Q.; Wu, W. C.; Chen, C. Y.; Jang, S. H.; Zhang, M.; Strovas, T.; Anderson, J.; Cookson, B.; Li, Y. Z.; Meldrum, D.; Chen, W. C.; Jen, A. K. Y. *J. Biomed. Mater. Res., Part A* **2010**, *93A*, 1068−1079.
(22) Sakurai, H.; Ritonga, M. T. S.; Shibatani, H.; Hirao, T. *J. Org. Chem.* **2005**, *70*, 2754−2762.
(23) Neto, B. A. D.; Carvalho, P. H. P. R.; Santos, D. C. B. D.; Gatto, C. C.; Ramos, L. M.; de Vasconcelos, N. M.; Corrêa, J. R.; Costa, M. B.; de Oliveira, H. C. B.; Silva, R. G. *RSC Adv.* **2012**, *2*, 1524−1532.
(24) Neto, B. A. D.; Correa, J. R.; Carvalho, P.; Santos, D.; Guido, B. C.; Gatto, C. C.; de Oliveira, H. C. B.; Fasciotti, M.; Eberlin, M. N.; da Silva, E. N. *J. Braz. Chem. Soc.* **2012**, *23*, 770−781.
(25) Oliveira, F. F. D.; Santos, D.; Lapis, A. A. M.; Correa, J. R.; Gomes, A. F.; Gozzo, F. C.; Moreira, P. F.; de Oliveira, V. C.; Quina, F. H.; Neto, B. A. D. *Bioorg. Med. Chem. Lett.* **2010**, *20*, 6001−6007.
(26) Netz, P. A. *Int. J. Quantum Chem.* **2012**, *112*, 3296−3302.
(27) Beaujuge, P. M.; Tsao, H. N.; Hansen, M. R.; Amb, C. M.; Risko, C.; Subbiah, J.; Choudhury, K. R.; Mavrinskiy, A.; Pisula, W.; Bredas, J. L.; So, F.; Mullen, K.; Reynolds, J. R. *J. Am. Chem. Soc.* **2012**, *134*, 8944−8957.

DOI: 10.1021/acs.joc.6b00245
J. Org. Chem. 2016, 81, 2958−2965

(28) Polander, L. E.; Pandey, L.; Barlow, S.; Tiwari, P.; Risko, C.; Kippelen, B.; Bredas, J. L.; Marder, S. R. *J. Phys. Chem. C* **2011**, *115*, 23149−23163.
(29) Pina, J.; de Melo, J. S.; Breusov, D.; Scherf, U. *Phys. Chem. Chem. Phys.* **2013**, *15*, 15204−15213.
(30) Lopes, T. O.; da Silva Filho, D. A.; Lapis, A. A. M.; de Oliveira, H. C. B.; Neto, B. A. D. *J. Phys. Org. Chem.* **2014**, *27*, 303−309.
(31) Consorti, C. S.; Ebeling, G.; Rodembusch, F.; Stefani, V.; Livotto, P. R.; Rominger, F.; Quina, F. H.; Yihwa, C.; Dupont, J. *Inorg. Chem.* **2004**, *43*, 530−536.
(32) Kumar, V.; Kumar, A.; Diwan, U.; Shweta, R.; Srivastava, S. K.; Upadhyay, K. K. *Sens. Actuators, B* **2015**, *207*, 650−657.
(33) Kwok, W. M.; Ma, C.; Phillips, D.; Matousek, P.; Parker, A. W.; Towrie, M. *J. Phys. Chem. A* **2000**, *104*, 4188−4197.
(34) Fayed, T. A.; El-Morsi, M. A.; El-Nahass, M. N. *J. Photochem. Photobiol., A* **2011**, *224*, 38−45.
(35) Wu, J.; Lai, G.; Li, Z.; Lu, Y.; Leng, T.; Shen, Y.; Wang, C. *Dyes Pigm.* **2016**, *124*, 268−276.
(36) Ishi-i, T.; Kitahara, I.; Yamada, S.; Sanada, Y.; Sakurai, K.; Tanaka, A.; Hasebe, N.; Yoshihara, T.; Tobita, S. *Org. Biomol. Chem.* **2015**, *13*, 1818−1828.
(37) Gautam, P.; Maragani, R.; Misra, R. *RSC Adv.* **2015**, *5*, 18288−18294.
(38) Belfield, K. D.; Bondar, M. V.; Yao, S.; Mikhailov, I. A.; Polikanov, V. S.; Przhonska, O. V. *J. Phys. Chem. C* **2014**, *118*, 13790−13800.
(39) Zhan, R.; Liu, B. *Macromol. Chem. Phys.* **2015**, *216*, 131−144.
(40) Parker, T. C.; Patel, D. G.; Moudgil, K.; Barlow, S.; Risko, C.; Bredas, J.-L.; Reynolds, J. R.; Marder, S. R. *Mater. Horiz.* **2015**, *2*, 22−36.
(41) Bolisetty, M.; Li, C. T.; Thomas, K. R. J.; Bodedla, G. B.; Ho, K. C. *Tetrahedron* **2015**, *71*, 4203−4212.
(42) Bashirov, D. A.; Sukhikh, T. S.; Kuratieva, N. V.; Chulanova, E. A.; Yushina, I. V.; Gritsan, N. P.; Konchenko, S. N.; Zibarev, A. V. *RSC Adv.* **2014**, *4*, 28309−28316.
(43) Sonar, P.; Williams, E. L.; Singh, S. P.; Manzhos, S.; Dodabalapur, A. *Phys. Chem. Chem. Phys.* **2013**, *15*, 17064−17069.
(44) Ruan, Y.-B.; Yu, Y.; Li, C.; Bogliotti, N.; Tang, J.; Xie, J. *Tetrahedron* **2013**, *69*, 4603−4608.
(45) Misra, R.; Gautam, P.; Mobin, S. M. *J. Org. Chem.* **2013**, *78*, 12440−12452.
(46) Laurent, A. D.; Houari, Y.; Carvalho, P. H. P. R.; Neto, B. A. D.; Jacquemin, D. *RSC Adv.* **2014**, *4*, 14189−14192.
(47) Saravanan, C.; Easwaramoorthi, S.; Hsiow, C.-Y.; Wang, K.; Hayashi, M.; Wang, L. *Org. Lett.* **2014**, *16*, 354−357.
(48) Steiner, T. *Angew. Chem., Int. Ed.* **2002**, *41*, 48−76.
(49) Akhtaruzzaman, M.; Tomura, M.; Nishida, J.; Yamashita, Y. *J. Org. Chem.* **2004**, *69*, 2953−2958.
(50) Shanan-Atidi, H.; Bar-Eli, K. H. *J. Phys. Chem.* **1970**, *74*, 961−963.
(51) Paul, B. K.; Samanta, A.; Guchhait, N. *J. Fluoresc.* **2011**, *21*, 1265−1279.
(52) Ulrich, G.; Nastasi, F.; Retailleau, P.; Puntoriero, F.; Ziessel, R.; Campagna, S. *Chem. - Eur. J.* **2008**, *14*, 4381−4392.
(53) Khan, A. U.; Kasha, M. *Proc. Natl. Acad. Sci. U. S. A.* **1983**, *80*, 1767−1770.
(54) Ravi, M.; Soujanya, T.; Samanta, A.; Radhakrishnan, T. P. *J. Chem. Soc., Faraday Trans.* **1995**, *91*, 2739−2742.
(55) Reichardt, C. *Chem. Rev.* **1994**, *94*, 2319−2358.

DOI: 10.1021/acs.joc.6b00245
J. Org. Chem. 2016, 81, 2958−2965